Pattern Formation and Transport for Externally Driven Active Matter on Periodic Substrates

C. Reichhardt and C. J. O. Reichhardt

Theoretical Division and Center for Nonlinear Studies, Los Alamos National Laboratory, Los Alamos, New Mexico 87545, USA

arXiv:2301.08380v1 [cond-mat.soft] 20 Jan 2023

Abstract – We investigate the transport of interacting active run-and-tumble particles moving under an external drift force through a periodic array of obstacles for increasing drive amplitudes. For high activity where the system forms a motility induced phase separated state, there are several distinct dynamic phases including a low drive pinned cluster phase, an intermediate uniform fluid, and a higher drive stripe crystal state. The transitions between the phases are correlated with signatures in the transport curves, differential mobility, and power spectra of the velocity fluctuations. In contrast, in the low activity regime the transport curves and power spectra undergo little change as a function of drive. We argue that in the high activity limit, the behavior is similar to that of driven solids on periodic substrates, while in the low activity limit the system behaves like a driven fluid.

Introduction. – There is a wide variety of systems that can be described as an assembly of interacting particles driven over a periodic substrate or arrays of obstacles [1]. Examples of this type of system include vortices in type-II superconductors [2–5], skyrmions [6], colloids [7, 8], Bose-Einstein condensates [9], liquid crystals [10], and frictional systems [11]. When solids or crystals are driven over a periodic substrate, distinct dynamical phases appear such as a low drive pinned state, a soliton state consisting of pinned and moving particles, plastically deforming states, fluidized states, and moving smectics [1,12–17]. Transitions between different moving states can be associated with distinct types of fluctuations and changes in velocity, leading to jumps or even dips in the velocity-force and differential mobility curves. In contrast, for fluids driven over periodic substrates, fewer features appear and the response is often linear with drive [1].

Another type of collective particle system that is currently being studied is active matter or self-driven particles [18–20]. In the absence of a substrate, such systems show interesting phenomena such as motility induced phase separation (MIPS), where the particles can self-cluster even when all of the particle-particle interactions are repulsive [21–26]. Once a substrate or wall is added, a variety of behaviors can appear that are not found in passive particle systems, including novel pressure effects [27], ratchet effects [28–31], and nucleation or wetting phases at walls or obstacles [32–34].

Active matter systems coupled to periodic substrates have been studied with a variety of simulations and experiments in both the single particle and collective limits [35–40]. Computational work on interacting systems has even shown that an active matter commensuration or Mott effect can occur in which for some fillings the active particles form an ordered MIPS state that is strongly pinned to the substrate, while for other fillings there is a more mobile active cluster glass phase [41]. In systems with random or periodic substrates, increasing the activity may initially improve the ability of active particles to move in response to an applied drift force, but once the activity becomes high enough to induce the formation of clustering phases, a clogging of the flow occurs [42, 43]. Most studies of interacting active matter on periodic substrates have been performed in the limit where there is either no drift force or where the external drift force is small; however, it is known from studies of nonactive systems such as driven solids on periodic substrates [1] that a variety of other flow phases are possible at higher drives.

In this work we consider collectively interacting active particles driven over a periodic substrate in both the high activity regime where the system forms a MIPS state and in the low activity or Brownian fluid regime. For high activity, at low drives the system is in an active clogged or pinned phase as previously observed [43], while with in-

creasing drive a depinning transition occurs into a uniform fluid, followed at high drives by a dynamical reordering into a phase separated stripe crystal. The onset of the different phases can be detected via peaks in the differential mobility as well as non-monotonic behavior of the clustering. We also show that velocity noise spectra can be used to characterize the dynamics. The velocity noise is large and of $1/f$ form in the coexistence regime near depinning, while the fluid phase and the stripe crystal states have low noise power with white noise characteristics. At low activities, the velocity-force curves rapidly become linear with increasing drive, the noise power is low, and there is a crossover from a two-dimensional (2D) liquid to a one-dimensional (1D) liquid at higher drives. We argue that in the high activity limit, the system behaves like a solid driven over a periodic array, whereas for low activity the system acts like a fluid with weak collective effects.

Model. – We consider a 2D assembly of repulsive disks with radius R_a that interact with a square array of obstacles, which are also modeled as repulsive disks with radius $R_{\rm obs}$. The system has periodic boundary conditions in the x and y directions, and the equation of motion for disk i is

$$\eta\frac{d\mathbf{r}_i}{dt} = \mathbf{F}^i_{\rm inter} + \mathbf{F}^i_{\rm sub} + \mathbf{F}^i_m + \mathbf{F}_D \ . \tag{1}$$

Here the velocity of the disk is $\mathbf{v}_i = d\mathbf{r}_i/dt$, the location of the disk is $\mathbf{r}_i$, and η_d is the damping force, which we set to $\eta_d = 1$. The particle-particle interaction forces $\mathbf{F}_{\rm inter}$ are given by short range harmonic repulsion, where we choose the interaction strength such that the overlap of interacting disks remains smaller than one percent of the disk radius. A similar interaction force $\mathbf{F}_{\rm obs}$ is used for the obstacles, which are modeled as fixed position harmonic disks placed in a square array with a lattice spacing of a. The motor force $\mathbf{F}_m$ represents run-and-tumble dynamics in which each active disk experiences a force of magnitude F_m applied in a randomly chosen direction during a run time of $\tau_{\rm run}$, after which the disk randomly reorients and moves in a different direction during the next running time interval. We characterize the system using the run length l_r, defined to be the distance a disk would move during a single run time in the absence of collisions with other disks or obstacles, $l_r = \tau_{\rm run}F_m$. The overall density of the system is the area underneath both the disks and the obstacles, $\phi = N_a\pi R_a^2/L^2 + N_{obs}\pi R_{\rm obs}/L^2$, where L is the size of each side of the simulation box. The driving force $\mathbf{F}_D = F_D\hat{\mathbf{x}}$ is applied in the x-direction. We measure the time series of the velocity fluctuations in the direction of drive, $V_x = \sum_i^{N_a}\mathbf{v}_i\cdot\hat{\mathbf{x}}$, as well as the time average of this quantity, $\langle V_x\rangle$. After applying a given drive F_D, we wait a fixed number of time steps before taking data in order to avoid any transient effects. We measure $\langle V_x\rangle$ as a function of varied F_D, allowing us to construct velocity-force curves similar to those studied for superconducting vortices, colloids, and frictional systems [1]. In this work we fix the disk radius to $R_a = 0.5$ and the obstacle radius to $R_{\rm obs} = 0.65$, and for most of the results the obstacle lattice constant is set to $a = 4.0$.

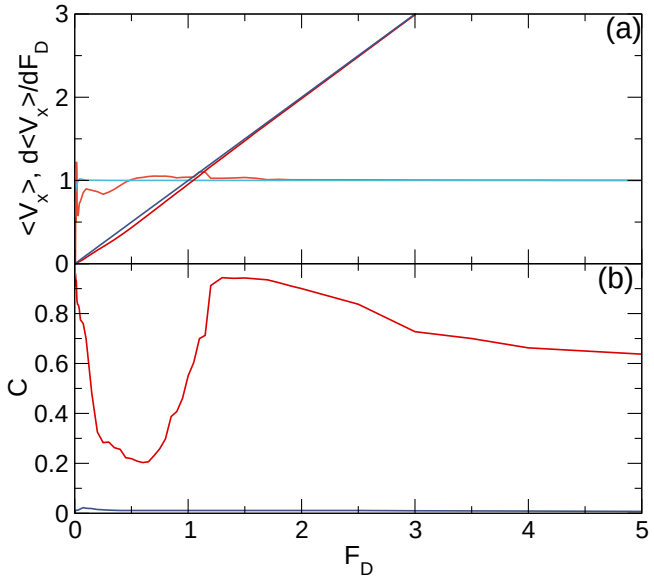


Fig. 1: (a) V_x (dark red and dark blue curves) and $d\langle V_x\rangle/dF_D$ (light red and light blue curves) vs F_D for run-and-tumble disks driven over a periodic square obstacle array for running lengths of $l_r = 0.02$ (dark and light blue) and $l_r = 180$ (dark and light red). Here $\phi = 0.5186$ and the obstacle lattice spacing $a = 4.0$. (b) The corresponding fraction C of particles in the largest cluster vs F_D.

Results. – We focus on the case where the total system density is $\phi = 0.5186$, well below the jamming density $\phi_J = 0.9$ of a passive system [44]. In the passive limit, there is no clogging or jamming effect and the velocity-force curves are linear for all values of F_D, so any deviation from linearity that we observe can be attributed to the activity. In Fig. 1(a) we plot $\langle V_x\rangle$ and $d\langle V\rangle_x/dF_D$ versus F_D for $l_r = 0.02$ in the low activity regime and $l_r = 180$ in the high activity regime. Figure 1(b) shows the size of the largest cluster C in the system, obtained by detecting particles that are in direct contact with each other. At $l_r = 0.02$, the behavior is similar to that of Brownian particles and the velocity-force curve has an almost completely linear dependence on F_D, while C is always small. For the high activity system, $\langle V_x\rangle$ is depressed below the low activity curve and the differential mobility $d\langle V_x\rangle/dF_D$ exhibits several spikes and jumps. The cluster measure C is also nonmonotonic and has a large value at low drives where the system forms a clogged state in which most particles have aggregated into a single cluster. There is a drop in C for $0.25 < F_D < 0.9$ when the system fluidizes, a peak in C near $F_D = 1.2$, and a slow decrease in C at higher drives when the system reaches a stripe crystal state.

To more clearly display the nonlinearity in the transport for the two regimes, in Fig. 2 we plot the same $d\langle V_x\rangle/dF_D$ versus F_D curves from Fig. 1 on a linear-log scale. The

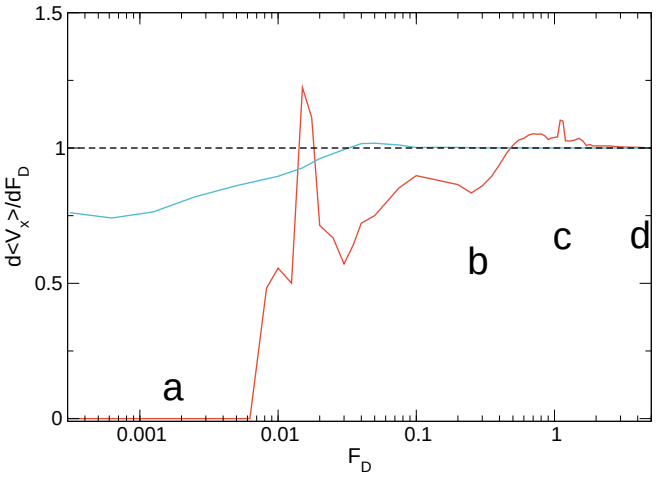


Fig. 2: A plot on a linear-log scale of $d\langle V_x\rangle/dF_D$ vs F_D from Fig. 1(a) at $\phi = 0.5186$ and $a = 4.0$ for $l_r = 0.02$ (light blue) and $l_r = 180$ (light red). The dashed line indicates the value of $d\langle V_x\rangle/dF_D$ that would appear for a linear velocity-force curve. The letters **a** through **d** indicate the values of F_D at which the images in Fig. 3 were obtained for the $l_r = 180$ sample.

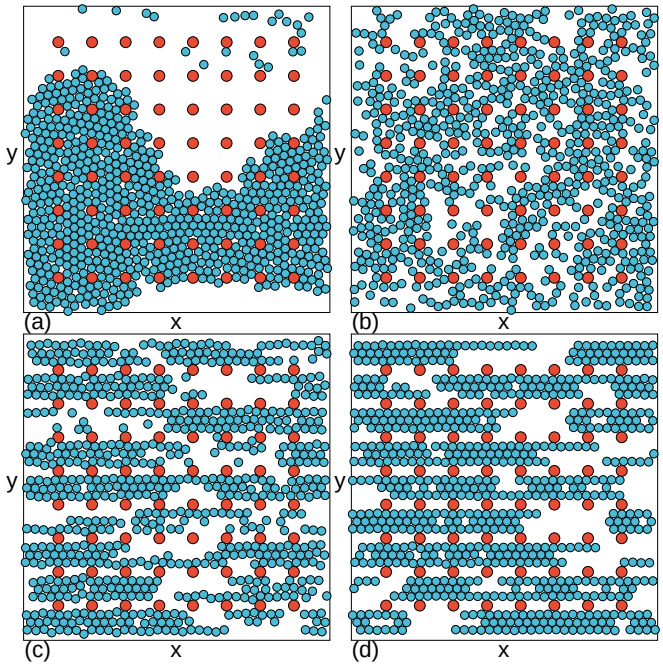


Fig. 3: The particle positions (blue circles) and obstacle locations (red circles) for the $l_r = 180$ system with $\phi = 0.5186$ and $a = 4.0$ at the drive values marked with letters in Fig. 2. (a) The clogged phase at $F_D = 0.0016$. (b) The fluid phase at $F_D = 0.3$. (c) The onset of density modulated stripe formation at $F_D = 1.0$. (d) The density modulated stripe crystal at $F_D = 5.0$.

dashed line indicates the expected result for a completely linear velocity-force curve, which is what we observe for $l_r = 0$ when the particles are passively driven between the obstacles. In the low activity regime, $d\langle V_x\rangle/dF_D$ is less than one for $F_D < 0.05$. Here the system forms a 2D fluid in which the particles move freely throughout space. In this state, when a finite drive F_D is applied, some of the particles become temporarily trapped behind the obstacles, leading to a reduction in $\langle V_x\rangle$ compared to the purely passive system. As F_D increases, this trapping effect is reduced, and for $F_D > 0.05$ the motion changes from 2D fluid flow to 1D channel flow in which all of the particles remain confined between adjacent rows of obstacles and the particle-obstacle interactions are minimized. For the high activity regime, there is a clogged phase for $F_D < 0.006$. This state is illustrated for $F_D = 0.0016$ in Fig. 3(a), where we highlight the mobile disk and obstacle positions. Here the particles form a single large system spanning cluster where the motion in the direction of drive is almost zero. This activity-induced clogged phase is similar to the one studied previously for active particles at a low drive on periodic substrates [41, 43]. Near $F_D = 0.01$, there is an effective depinning transition in which the clogged state breaks apart and the disks enter a moving fluid state, as shown in Fig. 3(b) at $F_D = 0.3$. Near $F_D = 1.0$, there is another peak in the $d\langle V_x\rangle/dF_D$ curve corresponding to a transition from the 2D fluid into a phase separated crystalline stripe phase, illustrated in Fig.3(c,d) for $F_D = 1.0$ and 5.0, respectively. At $F_D = 1.0$, there are some fluctuations in the structure and the stripes intermittently break apart and reform, while at $F_D = 5.0$, the stripes are stable. The stripes have an internal triangular crystalline ordering that is oriented in the driving direction.

In Fig. 4(a) we show the particle locations for the $l_r = 0.02$ low activity system from Fig. 2 at $F_D = 0.00125$ where the structure is a 2D fluid. At $F_D = 1.0$ in Fig. 4(b), the particles move in quasi-1D paths. Unlike the high activity case, the stripes remain liquidlike and there is no local crystalline ordering or density modulations in the direction of drive.

If the spacing a between the obstacles is varied, the depinning threshold can change and pass through maxima when an integer number of particles are able to fit exactly between the obstacles to form commensurate states. When we vary the total system density ϕ by changing the density of active particles, we find similar results in which there is a critical lowest density below which the high activity system can no longer form a clogged phase at low drives; however, the stripe cluster phase at higher drives is robust. Additional features can occur, such as the formation of stripes with an integer number of rows, as shown in Fig. 4(c) where the number of active particles in the system from Fig. 3 has been reduced to give a total density of $\phi = 0.2096$. Here, the system forms a series of 1D chains at $F_D = 5.0$. For larger obstacle spacings a, the stripes become more 2D in nature, as illustrated in Fig. 4(d) for a system with the same density $\phi = 0.5186$ as in Fig. 3 but with a increased to $a = 6.0$, where up to five rows of particles can fit between adjacent rows of obstacles.

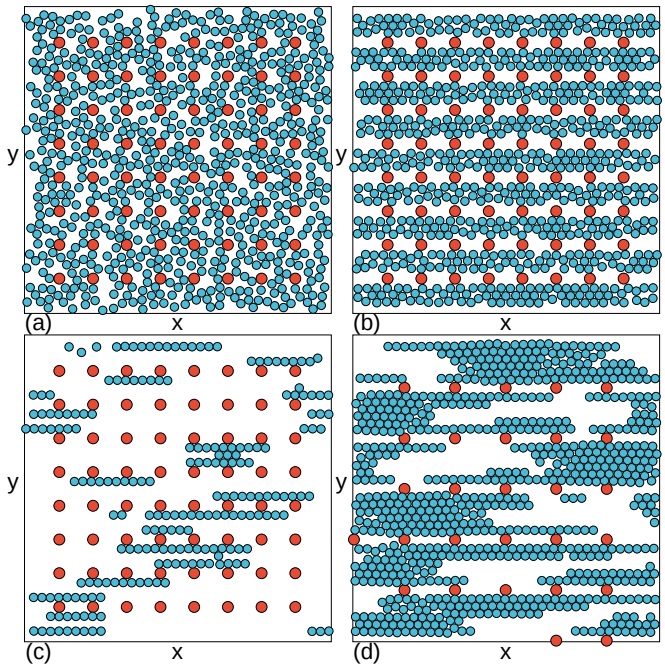


Fig. 4: The particle positions (blue circles) and obstacle locations (red circles) for the system from Fig. 2 with $\phi = 0.5186$ and $a = 4.0$. (a) $l_r = 0.02$ and $F_D = 0.00125$ in the 2D fluid phase. (b) $l_r = 0.02$ and $F_D = 1.0$ in the 1D fluid phase. (c) $l_r = 180$ at $F_D = 5.0$ in the stripe crystal phase at $\phi = 0.2096$ where the number of active particles has been reduced and the system forms 1D chains. (d) $l_r = 180$ at $F_D = 5.0$ in the stripe crystal regime at $\phi = 0.5186$ for a larger obstacle spacing of $a = 6.0$, where the stripes are more 2D in nature and contain up to five rows of particles each.

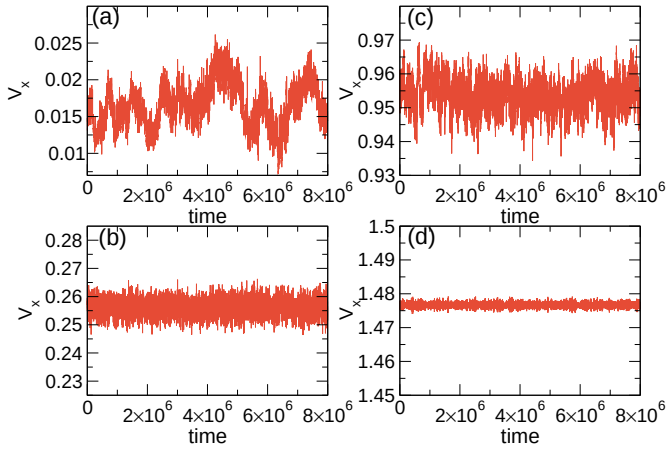


Fig. 5: The time series of the x-direction velocities V_x for the system with $l_r = 180$, $\phi = 0.5186$, and $a = 4.0$. (a) $F_D = 0.03$ just above the depinning transition from the clogged phase. (b) $F_D = 0.3$ in the fluid phase. (c) $F_D = 1.0$ where there is coexistence between the fluid and a stripe crystal. (d) $F_D = 1.5$ in the stripe crystal phase.

Another method to characterize depinning and sliding dynamics is by examining the velocity fluctuations and their power spectra. For example, during plastic depinning the velocity fluctuations can be quite large since large numbers of particles jump between pinned and moving states, whereas in a moving fluid state, the particles are continuously moving and the velocity fluctuations are small [1]. In Fig. 5 we plot time series of the x-direction velocities V_x for the highly active system at $F_D = 0.03$, 0.3, 1.0, and 1.5. For $F_D = 0.03$ in Fig. 5(a), the system is just above the depinning transition and there are strong velocity fluctuations. In Fig. 5(b) at $F_D = 0.3$, the system is in a fluid phase and the velocity fluctuations are less pronounced. At $F_D = 1.0$ in Fig. 5(c), the system is transitioning from the 2D fluid phase to a stripe crystal and there is coexistence between the two states, leading to enhanced velocity fluctuations, while in the stripe crystal phase at $F_D = 1.5$ in Fig. 5(d), the velocity fluctuations are strongly reduced.

To better characterize the changes in the velocity fluctuations, we compute the power spectrum of the velocity time series, $S(f) = |\int V_x(t)e^{-i2\pi ft}dt|$. In Fig. 6(a) we plot the noise power S_0 versus F_D at high and low activities. We obtain S_0 by integrating $S(f)$ over a narrow window around $f = 10$. The noise power is low for the low activity sample, while for high activity of $l_r = 180$, S_0 is non-monotonic. For $F_D < 0.0125$, which corresponds to the clogged phase in which there is almost no motion, S_0 is nearly zero. Over the range $0.0125 \leq F_D < 0.2$, the noise power is high and the system is in the depinned or plastic regime with a coexistence of pinned clusters and moving fluid. There is a drop of S_0 to a low value for $0.2 \leq F_D < 0.9$, corresponding to the fluid phase. Near $F_D = 1.0$, the noise power is high again in the coexistence regime of the fluid and cluster stripe phases, while S_0 is low in the stripe crystal state for $F_D > 1.0$.

From the behavior of the noise and transport features, we identify four dynamical phases in the high activity system. In phase I, the system is clogged with a large cluster and low mobility. Phase II is the region in which the fluctuating clogged fluid phase coexists with a fluid phase. The pure fluid state is phase III, and phase II_b is a coexistence between the fluid phase and the stripe crystal phase. Finally, at high drives, the stripe crystal phase IV emerges. Large values of the noise power are associated with the coexistence phases in which the system intermittently jumps between two distinct states. The low activity system exhibits only the 2D fluid phase III and phase IV_b, which is a 1D fluid. We can also examine the power spectra directly, as plotted in Fig. 6(b) for $F_D = 0.03$ in the strongly fluctuating depinned clogged state and $F_D = 0.3$ in the fluid phase. The dashed line is a fit to a power law, $S(f) \propto f^{\alpha}$ with exponent $\alpha = -1.3$, for the strongly fluctuating state. In non-active systems undergoing plastic depinning, typical velocity fluctuation power spectra have a power law form with an exponent in the range $-2.0 < \alpha < -1.0$ [1]. For the active system, we find that in the fluid state the velocity noise is fairly white and has

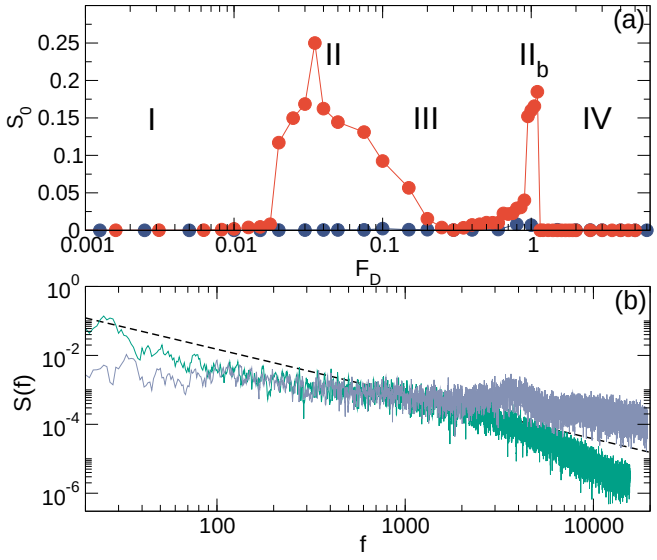


Fig. 6: (a) The noise power S_0 over a fixed frequency range vs F_D obtained from the power spectra of the velocity time series for samples with $\phi = 0.5186$ and $a = 4.0$ at a high activity of $l_r = 180$ (red) and a low activity of $l_r = 0.02$ (blue). For low activity, the noise power is always low. The dynamic phases are: I, clogged; II, coexistence between clogged and fluid; III, fluid; II$_b$, coexistence between fluid and stripe crystal; and IV, stripe crystal. (b) The power spectra $S(f)$ vs frequency f for the high activity $l_r = 180$ sample in phase II at $F_D = 0.03$ and in phase III at $F_D = 0.3$. The dashed line is a power law fit with exponent $\alpha = -1.3$.

an exponent α close to zero. Additionally, the fluid phase exhibits a characteristic peak at higher frequencies that arises when the periodicity of the substrate introduces a typical time between particle-obstacle collisions. In phase II$_b$ we also find broad band or power law noise, while the spectrum is white in phase IV.

The behavior of the high activity regime is similar to what is found for flexible solids of interacting particles, such as superconducting vortices or colloids, driven over periodic arrays, and exhibits similar peaks and dips in the differential mobility as well as peaks in the noise near the dynamical transitions [1]. In the active particle case, the solid emerges at high activities due to the MIPS mechanism, where the dense phase can be viewed as a solid with longer range correlations. In the low activity limit, the system acts like a weakly correlated fluid driven over a periodic substrate, where there are only short range correlations. It is likely that as the run length is decreased, the behavior would gradually change from solidlike to fluidlike.

Summary. – We have investigated the dynamics of active matter run-and-tumble disks moving through a periodic obstacle array under varied external drives. We consider the low activity or Brownian regime and the high activity or motility induced phase separation regime where clusters spontaneously form, and we focus on systems where the total density is well below the density at which jamming would occur for passive disks. For low activity, the velocity-force curves have a small nonlinear regime at low drives where the system forms a 2D fluid, followed by a crossover to a linear regime at higher drives where there is a 1D fluid flow state. The velocity noise power is low for all drives. At high activity, the transport curves are strongly nonlinear and have two peaks in the differential mobility. The first peak corresponds to a depinning transition from a clogged state to a flowing 2D fluid, and the second peak is associated with the transition from a fluid to a density modulated crystalline stripe phase. The moving stripe phase can display different patterns depending on the lattice spacing and the overall density of the system. The velocity noise power also passes through peaks at the transitions between the different flow states, and the velocity noise has a broad band or $1/f$ character in the coexistence regime between two phases but is white in the fluid phases. We argue that the high activity system behaves much like a solid depinning from a periodic substrate, and that the solid-like behavior arises due to the motility induced phase separation. In contrast, the low activity state behaves like a weakly correlated fluid.

* * *

We gratefully acknowledge the support of the U.S. Department of Energy through the LANL/LDRD program for this work. This work was supported by the US Department of Energy through the Los Alamos National Laboratory. Los Alamos National Laboratory is operated by Triad National Security, LLC, for the National Nuclear Security Administration of the U. S. Department of Energy (Contract No. 892333218NCA000001).

REFERENCES

[1] Reichhardt C. and Reichhardt C. J. O., *Rep. Prog. Phys.*, **80** (2017) 026501.
[2] Baert M., Metlushko V. V., Jonckheere R., Moshchalkov V. V. and Bruynseraede Y., *Phys. Rev. Lett.*, **74** (1995) 3269.
[3] Harada K., Kamimura O., Kasai H., Matsuda T., Tonomura A. and Moshchalkov V. V., *Science*, **274** (1996) 1167.
[4] Martín J. I., Vélez M., Nogués J. and Schuller I. K., *Phys. Rev. Lett.*, **79** (1997) 1929.
[5] Reichhardt C., Olson C. J. and Nori F., *Phys. Rev. B*, **58** (1998) 6534.
[6] Reichhardt C., Reichhardt C. J. O. and Milosevic M., *Rev. Mod. Phys.*, **94** (2022) 035005.
[7] Reichhardt C. and Olson C. J., *Phys. Rev. Lett.*, **88** (2002) 248301.
[8] Brunner M. and Bechinger C., *Phys. Rev. Lett.*, **88** (2002) 248302.
[9] Tung S., Schweikhard V. and Cornell E. A., *Phys. Rev. Lett.*, **97** (2006) 240402.
[10] Duzgun A., Nisoli C., Reichhardt C. J. O. and Reichhardt C., *Soft Matter*, **16** (2020) 3338.

[11] Vanossi A., Manini N., Urbakh M., Zapperi S. and Tosatti E., *Rev. Mod. Phys.*, **85** (2013) 529.

[12] Reichhardt C., Olson C. J. and Nori F., *Phys. Rev. Lett.*, **78** (1997) 2648.

[13] Gutierrez J., Silhanek A. V., Van de Vondel J., Gillijns W. and Moshchalkov V. V., *Phys. Rev. B*, **80** (2009) 140514.

[14] Bohlein T., Mikhael J. and Bechinger C., *Nature Mater.*, **11** (2012) 126.

[15] Vanossi A., Manini N. and Tosatti E., *Proc. Natl. Acad. Sci. (USA)*, **109** (2012) 16429.

[16] McDermott D., Amelang J., Reichhardt C. J. O. and Reichhardt C., *Phys. Rev. E*, **88** (2013) 062301.

[17] Hasnain J., Jungblut S., Tröster A. and Dellago C., *Nanoscale*, **6** (2014) 10161.

[18] Marchetti M. C., Joanny J. F., Ramaswamy S., Liverpool T. B., Prost J., Rao M. and Simha R. A., *Rev. Mod. Phys.*, **85** (2013) 1143.

[19] Bechinger C., Di Leonardo R., Löwen H., Reichhardt C., Volpe G. and Volpe G., *Rev. Mod. Phys.*, **88** (2016) 045006.

[20] Gompper G., Bechinger C., Stark H. and Winkler R. G., *Eur. Phys. J. E*, **44** (2021) 103.

[21] Fily Y. and Marchetti M. C., *Phys. Rev. Lett.*, **108** (2012) 235702.

[22] Redner G. S., Hagan M. F. and Baskaran A., *Phys. Rev. Lett.*, **110** (2013) 055701.

[23] Palacci J., Sacanna S., Steinberg A. P., Pine D. J. and Chaikin P. M., *Science*, **339** (2013) 936.

[24] Buttinoni I., Bialké J., Kümmel F., Löwen H., Bechinger C. and Speck T., *Phys. Rev. Lett.*, **110** (2013) 238301.

[25] Reichhardt C. and Reichhardt C. J. O., *Phys. Rev. E*, **91** (2015) 032313.

[26] Cates M. E. and Tailleur J., *Annual Review of Condensed Matter Physics*, **6** (2015) 219.

[27] Nikola N., Solon A. P., Kafri Y., Kardar M., Tailleur J. and Voituriez R., *Phys. Rev. Lett.*, **117** (2016) 098001.

[28] Di Leonardo R., Angelani L., Dell'Arciprete D., Ruocco G., Iebba V., Schippa S., Conte M. P., Mecarini F., De Angelis F. and Di Fabrizio E., *Proc. Natl. Acad. Sci. (USA)*, **107** (2010) 9541.

[29] Reichhardt C. and Reichhardt C. J. O., *Phys. Rev. E*, **88** (2013) 062310.

[30] Ai B.-Q. and Wu J.-C., *J. Chem. Phys.*, **140** (2014) 094103.

[31] Granek O., Kafri Y. and Tailleur J., *Phys. Rev. Lett.*, **129** (2022) 038001.

[32] Sándor C., Libál A., Reichhardt C. and Reichhardt C. J. O., *J. Chem. Phys.*, **146** (2017) 204903.

[33] Sepúlveda N. and Soto R., *Phys. Rev. Lett.*, **119** (2017) 078001.

[34] Neta P. D., Tasinkevych M., Telo da Gama M. M. and Dias C. S., *Soft Matter*, **17** (2021) 2468.

[35] Volpe G., Buttinoni I., Vogt D., Kümmerer H.-J. and Bechinger C., *Soft Matter*, **7** (2011) 8810.

[36] Reichhardt C. and Reichhardt C. J. O., *Phys. Rev. E*, **102** (2020) 042616.

[37] Brun-Cosme-Bruny M., Förtsch A., Zimmermann W., Bertin E., Peyla P. and Rafaï S., *Phys. Rev. Fluids*, **5** (2020) 093302.

[38] Reichhardt C., Libál A. and Reichhardt C. J. O., *EPL*, **139** (2022) 27001.

[39] Nabil M., Frankowski A., Orosa A., Fuller A. and Nourhani A., *Phys. Rev. E*, **105** (2022) 054610.

[40] Chopra P., Quint D., Gopinathan A. and Liu B., *Phys. Rev. Fluids*, **7** (2022) L071101.

[41] Reichhardt C. and Reichhardt C. J. O., *Phys. Rev. E*, **103** (2021) 022602.

[42] Reichhardt C. and Olson Reichhardt C. J., *Phys. Rev. E*, **90** (2014) 012701.

[43] Reichhardt C. and Reichhardt C. J. O., *Phys. Rev. E*, **103** (2021) 062603.

[44] Reichhardt C. and Reichhardt C. J. O., *Soft Matter*, **10** (2014) 2932.